

- [5] C.-P. Chen, K. Sugawara, Z. Ma, T. Anada, and D. W. P. Tomas, "Compact magnetic loop probe for microwave EM field-mapping and its applications in dielectric constant measurement," in *Proc. Eur. Microw. Conf.*, Oct. 2007, pp. 226–229.
- [6] N. Ando *et al.*, "Miniaturized thin-film magnetic field probe with high spatial resolution for LSI chip measurement," in *Proc. Int. Symp. Electromagn. Compat. (EMC)*, vol. 2, Aug. 2004, pp. 357–362.
- [7] N. Tamaki, N. Masuda, T. Kuriyama, J.-C. Bu, M. Yamaguchi, and K.-I. Arai, "A miniature thin-film shielded-loop probe with a flip-chip bonding for magnetic near field measurements," *Electron. Commun. Jpn.*, vol. 88, no. 4, pp. 37–45, 2005.
- [8] H.-H. Chuang *et al.*, "A magnetic-field resonant probe with enhanced sensitivity for RF interference applications," *IEEE Trans. Electromagn. Compat.*, vol. 55, no. 6, pp. 991–998, Dec. 2013.
- [9] Y.-T. Chou and H.-C. Lu, "Magnetic near-field probes with high-pass and notch filters for electric field suppression," *IEEE Trans. Microw. Theory Techn.*, vol. 61, no. 6, pp. 2460–2470, Jun. 2013.
- [10] W. H. Haydl, "On the use of vias in conductor-backed coplanar circuits," *IEEE Trans. Microw. Theory Techn.*, vol. 50, no. 6, pp. 1571–1577, Jun. 2002.
- [11] M. Yu, R. Vahldieck, and J. Huang, "Comparing coax launcher and wafer probe excitation for 10 mil conductor backed CPW with via holes and airbridges," in *IEEE MTT-S Int. Microw. Symp. Dig.*, vol. 2, Jun. 1993, pp. 705–708.
- [12] E. R. Pillai, "Coax via—A technique to reduce crosstalk and enhance impedance match at vias in high-frequency multilayer packages verified by FDTD and MoM modeling," *IEEE Trans. Microw. Theory Techn.*, vol. 45, no. 10, pp. 1981–1985, Oct. 1997.
- [13] T. Harada, H. Sasaki, and E. Hankui, "Time-domain magnetic field waveform measurement near printed circuit boards," *Elect. Eng. Jpn.*, vol. 125, no. 4, pp. 9–18, 1998.

## A Wideband High-Gain Cavity-Backed Low-Profile Dipole Antenna

Jian-Ying Li, Rui Xu, Xuan Zhang, Shi-Gang Zhou,  
and Guang-Wei Yang

**Abstract**—In this communication, a compact, wideband, low-profile, and high gain dipole antenna is proposed. A microstrip coupling line is used to feed the ellipse pairs, which is two arms of the antenna. This simple feeding structure can significantly enhance the impedance bandwidth (IBW). A cavity-backed structure is adopted to achieve the low-profile antenna. With the influence of the cavity-backed structure, the new antenna has a higher gain over the whole frequency band. An optimized antenna with a height of only  $0.17\lambda$  (where  $\lambda$  is the free space wavelength at the lowest frequency) is designed and measured. The measured result shows that the IBW for VSWR  $< 2$  is 117% (2.48–9.51 GHz). Further, the gain bandwidth (Gain  $> 6$  dBi) from 2.57 to 8.73 GHz is more than 108.9%. The antenna radiation pattern performs well over the whole band, and the peak gain can reach 11.8 dBi.

**Index Terms**—Broadband antenna, higher antenna gain, low-profile.

### I. INTRODUCTION

In recent years, with the rapid development of modern wireless communication technologies, such as 2G, 3G, Wi-Fi, and 4G LTE, and to meet the demand for simultaneous operation of such communication systems, compact ultrawideband low-profile antennas have attracted increasing attention. In addition to the above communication systems, low-profile wideband antennas are used in such applications as ground-penetrating radar, through-wall radar, medical imaging, and precision location systems. There is an intensive demand to design an antenna suitable for the modern wireless systems with a compact structure, a broad operating band, stable radiation patterns, and higher gain over the whole working frequency band.

The printed dipole [1] antenna, which includes a center-fed coplanar strip dipole, a double-sided printed dipole, and a folded printed dipole, has a compact size. Additionally, the planar printed-strip dipole antenna has many other advantages, such as easy fabrication, a broad bandwidth, lower surface wave excitation, and low cost. In [2], a printed fat dipole fed by a tapered microstrip balun is discussed, which has a wide bandwidth of 96% and little squint radiation patterns. Numerous antennas have been developed and are found in the literature [3]–[8]. In [3], the antenna is excited by a coaxial probe that works as a balun, limiting the antenna impedance bandwidth (IBW). The antennas in [4]–[7] are fed by a microstrip feed-line to achieve a broad bandwidth. In [7], the antenna profile is decreased to  $0.1\lambda$  (where  $\lambda$  is the free space wavelength at the lowest frequency), but the antenna gain is very low at lower frequencies. The antenna in [8] is fed by a coupling microstrip line with a simple structure. However, the radiation patterns of this antenna deteriorate at the high-frequency band, and the antenna height is a little bigger ( $0.24\lambda$ ). In [9], the antenna is excited by an air microstrip line embedded in the patch,

Manuscript received November 11, 2015; revised August 5, 2016; accepted September 2, 2016. Date of publication October 24, 2016; date of current version December 5, 2016. This work was supported in part by the National Natural Science Foundation of China under Grant 61271416 and Grant 61301093 and in part by the Fundamental Research Funds for the Central Universities under Grant GEKY8002.

The authors are with the School of Electronics and Information, Northwestern Polytechnical University, Xi'an 710072, China (e-mail: jianyngli@nwpu.edu.cn; rxuilj@163.com).

Color versions of one or more of the figures in this communication are available online at <http://ieeexplore.ieee.org>.

Digital Object Identifier 10.1109/TAP.2016.2620607

TABLE I  
COMPARISON OF MEASURED WIDEBAND LOW-PROFILE ANTENNAS

Ref.	Size (mm <sup>3</sup> ) $\lambda=C/f_{\text{Low}}$	VSWR<2 BW (% , GHz)	Peak Gain (dBi)
[3]	$0.78\lambda \times 0.78\lambda \times 0.13\lambda$	53.1 (1.8~3.1)	8.9
[4]	$0.60\lambda \times 0.60\lambda \times 0.19\lambda$	113.0 (1.15~4.07)	11.0
[7]	$0.66\lambda \times 0.43\lambda \times 0.10\lambda$	71.0 (0.99~2.08)	9.0
[8]	$0.90\lambda \times 0.40\lambda \times 0.24\lambda$	85.7 (3.0~7.5)	8.0
[9]	$0.52\lambda \times 0.52\lambda \times 0.14\lambda$	62.6 (2.16~4.13)	12.0
[10]	$\Phi 0.86\lambda \times 0.18\lambda$	91.4 (2.15~5.7)	9.5
[11]	$0.90\lambda \times 0.90\lambda \times 0.30\lambda$	118(2.81~10.92)	10.0
[12]	$0.76\lambda \times 0.61\lambda \times 0.07\lambda$	55.8(1.91~3.39)	6.9
Prop.	$0.52\lambda \times 0.52\lambda \times 0.17\lambda$	117.0 (2.48~9.51)	11.8

and the IBW is more than 60%. Although the above-mentioned antennas have different feeding systems, all of them are designed to obtain the property of broadband impedance matching bandwidth. Moreover, many kinds of bow-tie antennas have been introduced toward achieving impedance matching technique and higher gain over wideband. In [10], a cavity-backed bow-tie antenna is introduced to improve the radiation performance at higher frequency bands; the antenna has a circular ring that acts as a special reflector. A U-shaped, bow-tie, magnetoelectric dipole unidirectional antenna with a dual-layer horned reflector for ultrawideband applications is presented in [11]. The IBW can reach 118%; although it is wider, its size is large, with dimension of  $0.90\lambda \times 0.90\lambda \times 0.30\lambda$ . Another low-profile wideband planar antenna, consisting of two triangular shorted patches, two planar electric dipoles and a U-shaped reflector, is presented in [12]. The antenna profile is very low at less than  $0.1\lambda$ ; however, the IBW is relatively narrow at 55.8% (1.91–3.39 GHz).

In this communication, a compact, wideband, low-profile high-gain dipole antenna is proposed. A microstrip coupling line with a simple structure is used to feed the antenna to obtain a broadband IBW. A cavity-backed structure is adopted to improve the radiation performance. Compared with conventional planar-backed structures, the new antenna has higher gain and good radiation patterns over the whole frequency band. Table I shows a comparison of the proposed antenna with other wideband low-profile antennas [3], [4], [7]–[12] presented in recent literature. The comparison shows that this antenna has a broader IBW, smaller relative volume, and higher antenna gain.

This communication is organized as follows. Section I provides an introduction to wireless communication, radar systems, and the research on wideband, low-profile high-gain antennas. Section II describes and analyzes the design of the proposed wideband low-profile antenna. Section III presents the simulated and measured results for the designed antenna. Section IV provides the study conclusions.

## II. ANTENNA DESIGN AND ANALYSIS

### A. Antenna Design

The goal of this communication is to design a compact, wideband low-profile antenna with higher gain. Fig. 1 shows the geometry, top view, and side view of the proposed antenna, which has a center

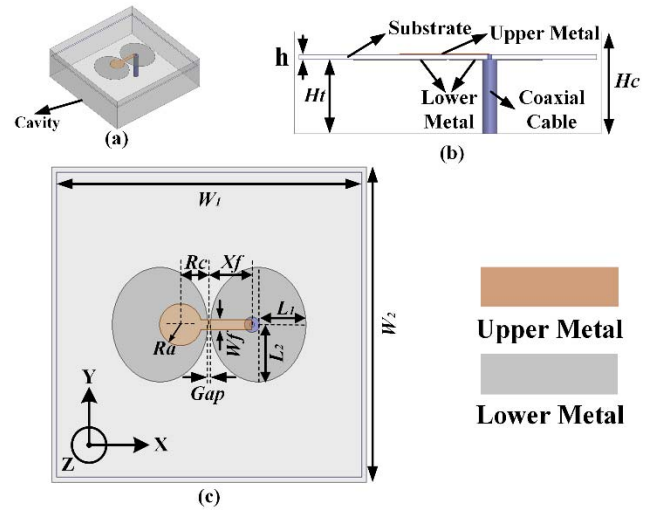


Fig. 1. Geometry of the proposed antenna (mm). (a) 3-D view. (b) Side view. (c) Top view.  $W_1 = 64.0$ ,  $W_2 = 66.0$ ,  $L_1 = 10.0$ ,  $L_2 = 12.0$ ,  $R_c = 6.0$ ,  $X_f = 9.0$ ,  $R_a = 4.4$ ,  $Gap = 0.6$ ,  $W_f = 2.0$ ,  $h = 1.0$ ,  $H_t = 16.0$ , and  $H_c = 22.0$ .

frequency of 5.77 GHz. The antenna consists of a substrate ( $\epsilon_r = 2.2$ ,  $\tan \delta = 0.0002$ , Rogers RT/duroid 5880), which is used to print the dipole antenna, and a cavity-backed reflector at the bottom of the antenna. The dimension of the substrate is  $64.0 \times 64.0 \times 1.0 \text{ mm}^3$ . A metal ellipse pair with short axis and long axis  $L_1$  and  $L_2$ , respectively, is printed on the lower surface of the substrate to serve as the dipole antenna; a 50- $\Omega$  microstrip transmission line fed by a coaxial cable is printed on the top surface of the substrate to be the feeding structure. The feeding point is  $(X_f, 0)$ . A metal circular patch, connected to the end of the 50- $\Omega$  microstrip transmission line, is used to improve the impedance matching. The center coordinates and radius of this circular patch are  $(-R_c, 0)$  and  $R_a$ , respectively. The inner pin of the SMA connector links directly to the 50- $\Omega$  microstrip transmission line, which is used to couple the left ellipse patch; and the outer conductor connects with the right ellipse patch. There is a small gap between the two ellipse patches ( $Gap$ ), which has a considerable effect on the impedance matching. This new feeding structure is similar to the Vivaldi antenna [11], [12] with a wider bandwidth. Therefore, a basic dipole antenna with a simple feeding structure is established. The antenna is located in a square cavity ( $66.0 \times 66.0 \times 22.0 \text{ mm}^3$ ). The distance ( $H_t$ ) between the lower surface of substrate and the bottom of the cavity is 16.0 mm. The lowest operating frequency  $F_L$  is mainly determined by the parameter  $L_1$ , which  $L_1$  determines the size of the dipole antenna. The lowest frequency  $F_L$  is roughly evaluated by applying the formula

$$F_L = \frac{300}{2(4L_1 + Gap)} \text{ (GHz)}. \quad (1)$$

The length is given in millimeters. The effect of other geometric parameters (such as  $L_2$  and  $R_c$ ) on the frequency range is not clear.

Fig. 2 shows the current distribution (at 3.0, 5.0, 7.0, and 9.0 GHz) on the surface of the antenna radiating element. At 3.0 and 7.0 GHz, the surface current of the antenna is mainly concentrated in the gap, and the current direction is along the  $x$ -axis. In contrast, at 5.0 and 9.0 GHz, the surface current of the antenna is not mainly concentrated in the gap, and the current direction is not mainly along the  $x$ -axis. The surface currents are also generated along  $y$ -axis or other directions, which offset with each other. In addition, the current intensity on the ellipse surface is lower when the antenna is operating

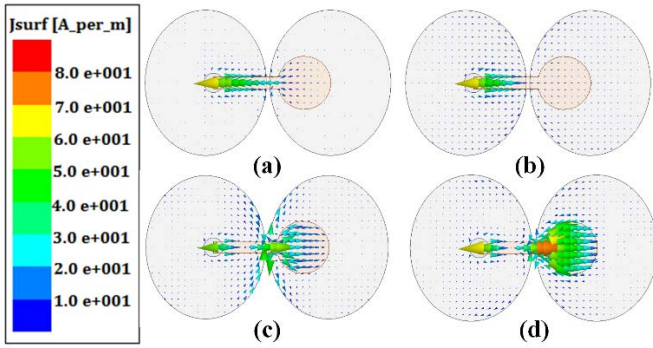


Fig. 2. Current distribution at (a) 3.0, (b) 5.0, (c) 7.0, and (d) 9.0 GHz.

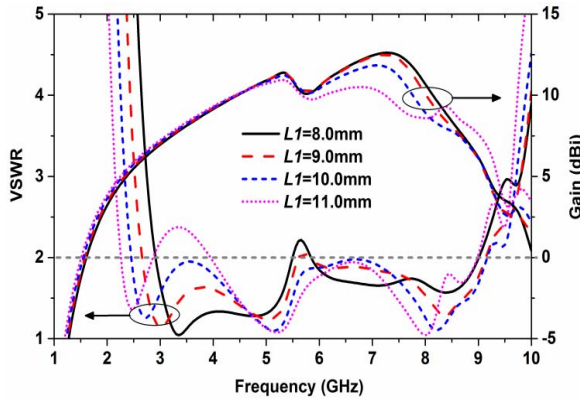


Fig. 3. Effects of various  $L_1$  on VSWR and gain (mm).  $W_1 = 64.0$ ,  $W_2 = 66.0$ ,  $L_2 = 12.0$ ,  $R_C = 6.0$ ,  $X_f = 9.0$ ,  $R_a = 4.4$ ,  $Gap = 0.6$ ,  $W_f = 2.0$ ,  $h = 1.0$ ,  $H_t = 16.0$ , and  $H_c = 22.0$ .

at 5.0 and 9.0 GHz, because the coupling between the two printed ellipses is stronger at 5.0 and 9.0 GHz. As a result of this current distribution, a down-warp of the patterns occurs and the peak gain of the antenna decreases at these frequency points (5.0 and 9.0 GHz).

**B. Parameters Studies**

To describe the performance of the antenna clearly, some key parameters of the designed antenna are discussed. All simulations in this communication are carried out by using the Ansoft high frequency structure simulation based on the finite-element method. The performance of the proposed antenna is determined by several important parameters, including the short axis of the ellipse ( $L_1$ ), the ratio of the ellipse ( $L_2/L_1$ ), the distance between two the ellipses ( $Gap$ ), and the height between the substrate and the square cavity ( $H_t$ ).

The first parameter studied is  $L_1$ , which has a considerable effect on the lowest frequency of the antenna. According to the simulated dates shown in Fig. 3, the antenna peak gain decreases as  $L_1$  increasing from 8.0 to 11.0 mm. When  $L_1$  is increased, the resonance of the VSWR clearly shifts to a lower frequency. However, when  $L_1$  is 11.0 mm, the VSWR deteriorates markedly at lower frequencies. The VSWR provides the best performance when  $L_1$  is 10.0 mm. The influence of  $L_1$  on the antenna is consistent with the antenna design theory.

The second parameter investigated is the ratio of the ellipses ( $L_2/L_1$ ). In the simulation results shown in Fig. 4, both the VSWR and gain curves are extended as this ratio changes from 1.0 to 1.4 ( $L_1 = 10.0$  mm;  $L_2 = 12.0, 14.4,$  and  $16.8$  mm). The VSWR curve deteriorates at 5.5 GHz, and the antenna peak gain decreases quickly

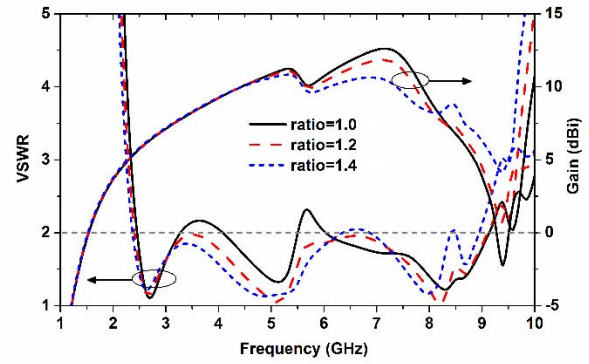


Fig. 4. Effects of various  $ratio$  on VSWR and gain (mm).  $W_1 = 64.0$ ,  $W_2 = 66.0$ ,  $L_1 = 10.0$ ,  $R_C = 6.0$ ,  $X_f = 9.0$ ,  $R_a = 4.4$ ,  $Gap = 0.6$ ,  $W_f = 2.0$ ,  $h = 1.0$ ,  $H_t = 16.0$ , and  $H_c = 22.0$ .

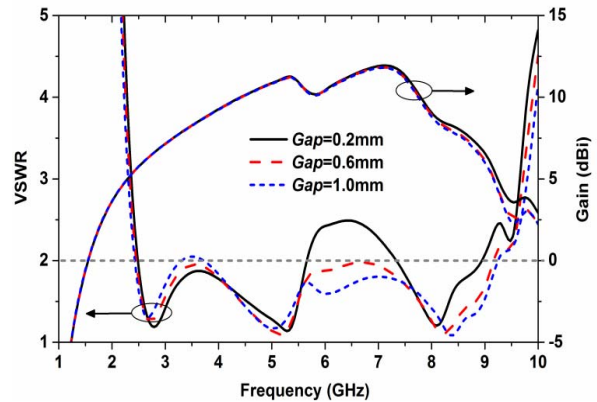


Fig. 5. Effects of various  $Gap$  on VSWR and gain (mm).  $W_1 = 64.0$ ,  $W_2 = 66.0$ ,  $L_1 = 10.0$ ,  $L_2 = 12.0$ ,  $R_C = 6.0$ ,  $X_f = 9.0$ ,  $R_a = 4.4$ ,  $W_f = 2.0$ ,  $h = 1.0$ ,  $H_t = 16.0$ , and  $H_c = 22.0$ .

when the ratio is 1.0. Although the antenna gain is increased at high frequency (8.0–9.0 GHz) when ratio is 1.4, the VSWR deteriorates markedly at high frequency, and the peak gain decreases to about 3.0 dB. The proper ratio is 1.2, at which the impedance matching is good, and the antenna gain is stable at high frequency.

The third parameter studied is the distance between the two ellipses ( $Gap$ ). Fig. 5 shows the influence of  $Gap$  on the performance of the antenna. The simulated date indicates that  $Gap$  mainly affects the antenna IBW and has little effect on the antenna gain. When  $Gap$  is 0.2 mm, the VSWR deteriorates markedly at middle frequency (6.3 GHz). On the contrary, when  $Gap$  increases to 1.0 mm, the VSWR deteriorates considerably at low frequency (3.5 GHz). When  $Gap$  is a proper value (0.6 mm), the VSWR performs well.

The last parameter studied is the height between the substrate and the square cavity ( $H_t$ ). Compared with the antenna without a cavity, the peak gain of the antenna with a cavity is clearly improved. As shown in Fig. 6, the maximum gain is increased by about 10 dBi at 7.5 GHz. The cavity-backed structure can obtain stable directional radiation patterns and stable gain over the whole operating band range. The height of the cavity-backed reflector determines the reflection frequency of the antenna; when  $H_t$  increases from 14.0 to 18.0 mm, the peak gain shifts to lower frequencies. When  $H_t$  is 14.0 mm, the gain curve at high frequency is very good; however, the VSWR deteriorates; when  $H_t$  is 18.0 mm, the antenna peak gain

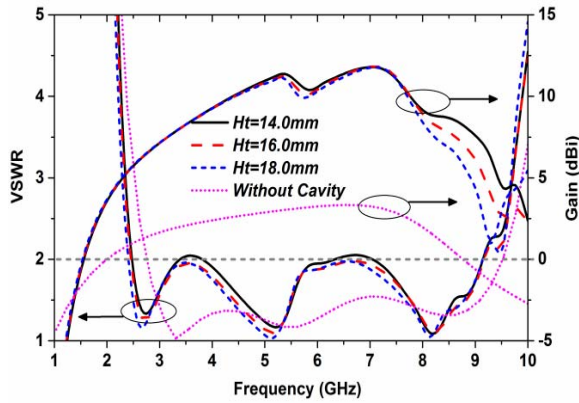


Fig. 6. Effects of various  $H_t$  on VSWR and gain (mm).  $W_1 = 64.0$ ,  $W_2 = 66.0$ ,  $L_1 = 10.0$ ,  $L_2 = 12.0$ ,  $R_C = 6.0$ ,  $X_f = 9.0$ ,  $R_a = 4.4$ ,  $Gap = 0.6$ ,  $W_f = 2.0$ ,  $h = 1.0$ , and  $H_c = 22.0$ .

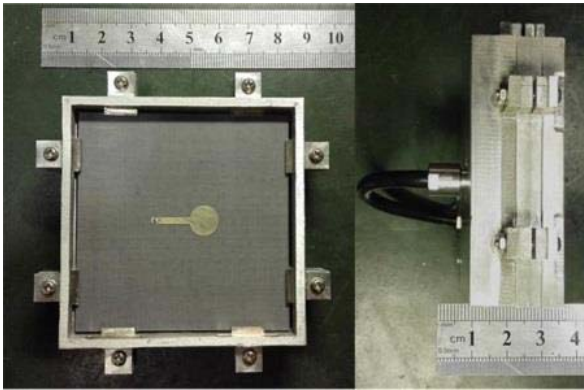


Fig. 7. Photograph of proposed antenna.

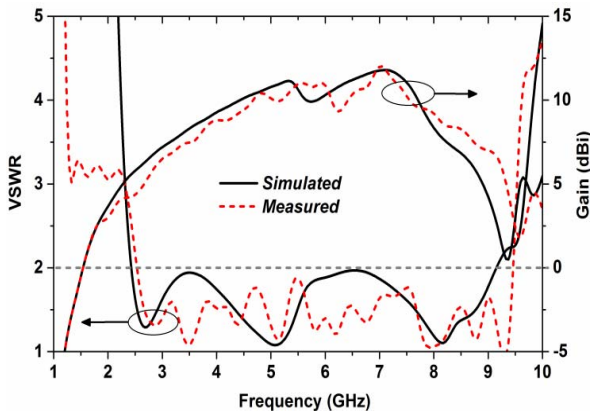


Fig. 8. Simulated and measured  $S_{11}$  of proposed antenna.

decreases greatly at high frequencies (7.5–9.0 GHz). Because this is a wideband antenna,  $H_t$  is about  $0.13\lambda$  (where  $\lambda$  is the free space wavelength at the lowest frequency, 2.48 GHz). In fact,  $H_t$  is about  $0.25\lambda$  at middle frequency (where  $\lambda$  is the free space wavelength at the middle frequency, 5.0 GHz). To achieve a high gain performance at high frequencies,  $H_t$  is selected to be 16.0 mm.

### III. EXPERIMENTAL RESULTS

The antenna is fabricated based on optimized design parameters. Fig. 7 shows the photograph of the antenna, and Fig. 8 presents both

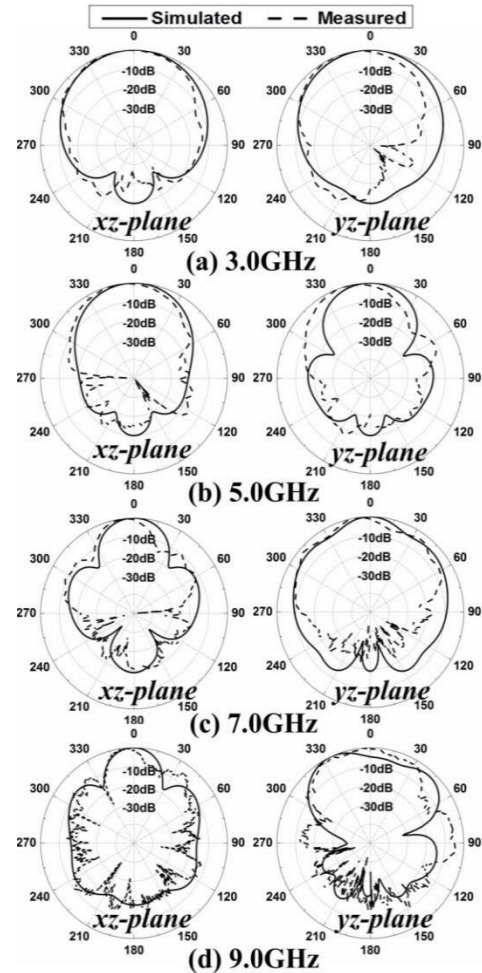


Fig. 9. Simulated and measured radiation patterns of proposed antenna. (a) 3.0 GHz. (b) 5.0 GHz. (c) 7.0 GHz. (d) 9.0 GHz.

the measured and the simulated values of VSWR and antenna gain. The measured results agree well with the simulated results and are slightly shifted to high frequencies. The measured IBW for VSWR  $< 2$  is 117.3% (2.48–9.51 GHz), whereas the simulated bandwidth is 108.9% (2.38–9.16 GHz). The designed antenna provides a very wide IBW and a very wide gain bandwidth of more than 108.9% (Gain  $> 6$  dBi) from 2.57 to 8.73 GHz. The peak gain can reach 11.8 dBi. Due to the coupling of the current distribution on the antenna surface, as shown in Fig. 2, the gain curve shows a drop near the middle frequency (5.0–6.0 GHz) and decreases quickly at high frequency.

Fig. 9 shows the simulated and the measured radiation patterns in  $xz$ -plane and  $yz$ -plane at 3.0, 5.0, 7.0, and 9.0 GHz. The radiation patterns are computed at selected frequencies that cover almost the entire operating band. The radiation patterns under test and simulation results are shown to be basically identical, except a slight deviation at 9 GHz. In  $xz$ -plane and  $yz$ -plane, the broadside radiation patterns are stable over the operating frequency band. The antenna patterns are consistent with the analysis results on the antenna surface current distribution, which is shown in Fig. 2. A down-warp of the patterns occurs at 5.0 and 9.0 GHz.

### IV. CONCLUSION

A novel wideband low-profile planar antenna with ellipse patches is presented in this communication. The compact low-profile antenna

has a pretty simple coupling feeding structure and higher gain. The IBW (VSWR < 2) of this antenna is 117.3% (2.48–9.51 GHz) and its height is only 22.0 mm ( $0.17\lambda_{\max}$ ). The antenna gain can maintain more than 6.0 dBi (108.9%, 2.57–8.73 GHz) and stable unidirectional radiation patterns. Parametric studies are carried out to optimize the antenna's dimensions to further understanding of its operating principles. The proposed antenna fully meets the requirements of 4G LTE communication systems.

## REFERENCES

- [1] P. Garg, P. Bhartia, I. Bahl, and A. Ittipiboon, *Microstrip Antenna Design Handbook*. Norwood, MA, USA: Artech House, 2001.
- [2] J. I. Kim, J. M. Kim, Y. J. Yoon, and C. S. Pyo, "Wideband printed fat dipole fed by tapered microstrip balun," in *Proc. IEEE Antennas Propag. Soc. Int. Symp. (APSUPEI)*, vol. 3, Jun. 2003, pp. 32–35.
- [3] L. Ge and K. M. Luk, "A magneto-electric dipole antenna with low-profile and simple structure," *IEEE Antennas Wireless Propag. Lett.*, vol. 12, pp. 140–142, 2013.
- [4] Z. Wang, J. Wu, Y. Yin, and X. Liu, "A broadband dual-element folded dipole antenna with a reflector," *IEEE Antennas Wireless Propag. Lett.*, vol. 13, pp. 750–753, 2014.
- [5] T.-G. Ma and S.-K. Jeng, "A printed dipole antenna with tapered slot feed for ultrawide-band applications," *IEEE Trans. Antennas Propag.*, vol. 53, no. 11, pp. 3833–3836, Nov. 2005.
- [6] Z. Zhou, S. Yang, and Z. Nie, "A novel broadband printed dipole antenna with low cross-polarization," *IEEE Trans. Antennas Propag.*, vol. 55, no. 11, pp. 3091–3093, Nov. 2007.
- [7] S.-G. Zhou and J.-Y. Li, "Low-profile and wideband antenna," *IEEE Antennas Wireless Propag. Lett.*, vol. 10, pp. 373–376, 2011.
- [8] J.-Y. Li, "Compact size dipole antenna," *Electron. Lett.*, vol. 44, no. 21, pp. 1229–1231, Oct. 2008.
- [9] H. Wong, K. M. Mak, and K. M. Luk, "Wideband shorted bowtie patch antenna with electric dipole," *IEEE Trans. Antennas Propag.*, vol. 56, no. 7, pp. 2098–2101, Jul. 2008.
- [10] S. W. Qu, J. L. Li, Q. Xue, and C. H. Chan, "Wideband cavity-backed bowtie antenna with pattern improvement," *IEEE Trans. Antennas Propag.*, vol. 56, no. 12, pp. 3850–3854, Dec. 2008.
- [11] B. Feng, S. Li, W. An, S. Yin, J. Li, and T. Qiu, "U-shaped bow-tie magneto-electric dipole antenna with a modified horned reflector for ultra-wideband applications," *IET Microw., Antennas Propag.*, vol. 8, no. 12, pp. 990–998, Sep. 2014.
- [12] M. Li and K.-M. Luk, "A low-profile wideband planar antenna," *IEEE Trans. Antennas Propag.*, vol. 61, no. 9, pp. 4411–4418, Sep. 2013.
- [13] O. Javashvili and D. Andersson, "New method for design implementation of Vivaldi antennas to improve its UWB behaviour," in *Proc. Antennas Propag. (EuCAP)*, Apr. 2010, pp. 1–5.
- [14] M. Manteghi and Y. Rahmat-Samii, "A novel UWB feeding mechanism for the TEM horn antenna, reflector IRA, and the Vivaldi antenna," *IEEE Antennas Propag. Mag.*, vol. 46, no. 5, pp. 81–87, Oct. 2004.

## Enhancement of Radiation With Irregular Wire Media

Sergei Yu. Kosulnikov, Mohammad S. Mirmoosa,  
Dmytro A. Vovchuk, Sergei A. Tretyakov,  
Stanislav B. Glybovski, and  
Constantin R. Simovski

**Abstract**—In this communication, we show that broadband enhancement of radiation from subwavelength sources can be achieved by using a new type of metamaterials—irregular random wire media. In contrast to samples of aligned metal wires, which give a narrow-band enhancement at Fabry–Perot resonances, here, the broadband enhancement is achieved due to the internal structure of the sample. Next, in contrast to lenses and hyperlenses, the proposed structure offers this enhancement without enlargement of the radiating aperture.

**Index Terms**—Gain control, periodic structures, radiation effects.

## I. INTRODUCTION

Wire media (WM) formed by electromagnetically dense arrays of metal wires attracted much attention in recent literature (see [1]) due to a variety of their applications such as enhanced heat-electricity conversion [2]–[4], subwavelength imaging [5], and some others [1]. Among useful properties of WM, there is enhancement of radiation from subwavelength electric and magnetic dipoles embedded into a WM. This effect has been studied in [6]–[9] and its qualitative measure is called the Purcell factor ( $F_P$ ). Tuning the parameters of WM one can achieve the very broadband and high Purcell factor  $F_P$ . This property is a consequence of the extraordinary anisotropy of WM [6] and/or strong spatial dispersion [8].

In known studies of the Purcell effect in WM [6]–[8], WM are regular arrays of coaligned wires embedded into a dielectric matrix, and here we call such structures *regular WM* (RWM). Though the Purcell factor of a RWM sample is high beyond the sample dimensional resonances, radiated power is mostly confined inside the finite WM sample due to total internal reflections [7] and can be strongly absorbed in the WM sample [8]. Therefore, one distinguishes between the so-called radiative Purcell factor  $F_{PR}$  and the total Purcell factor  $F_P$ . At microwaves the losses in copper or aluminum wires are small and the Purcell effect is mediated by the internal reflections. Then the regime  $F_{PR} \approx F_P \gg 1$  for a sample of RWM is achievable only at the Fabry–Perot resonances of the WM sample [7].

In order to free the power of a dipole field trapped inside a block of parallel wires in [10] and [11], we suggested to replace parallel

Manuscript received February 10, 2016; revised August 9, 2016; accepted August 20, 2016. Date of publication September 7, 2016; date of current version December 5, 2016. This work was supported by the Russian Science Foundation under Project 15-19-20054.

S. Yu. Kosulnikov and C. R. Simovski are with the Department of Radio Science and Engineering, Aalto University, 00076 Aalto, Finland, and also with ITMO University, 197101 Saint Petersburg, Russia (e-mail: sergei.2.kosulnikov@aalto.fi; konstantin.simovski@aalto.fi).

M. S. Mirmoosa and S. A. Tretyakov are with the Department of Radio Science and Engineering, Aalto University, 00076 Aalto, Finland (e-mail: mohammad.mirmoosa@aalto.fi; sergei.tretyakov@aalto.fi).

D. A. Vovchuk is with the Department of Radio Engineering and Information Security, Yuriy Fedkovych Chernivtsi National University, 58000 Chernivtsi, Ukraine (e-mail: dimavovchuk@gmail.com).

S. B. Glybovski is with ITMO University, 197101 Saint Petersburg, Russia (e-mail: s.glybovski@metalab.ifmo.ru).

Color versions of one or more of the figures in this communication are available online at <http://ieeexplore.ieee.org>.

Digital Object Identifier 10.1109/TAP.2016.2606569